POLITECNICO DI TORINO
Repository ISTITUZIONALE

Impact of the Overall Electrical Filter Shaping in Next-Generation 25 and 50 Gb/s PONs

Original
Impact of the Overall Electrical Filter Shaping in Next-Generation 25 and 50 Gb/s PONs / TORRES FERRERA, Pablo; Ferrero, Valter; Valvo, Maurizio; Gaudino, Roberto. - In: JOURNAL OF OPTICAL COMMUNICATIONS AND NETWORKING. - ISSN 1943-0620. - STAMPA. - 10:5(2018), pp. 493-505. [10.1364/JOCN.10.000493]

Availability:
This version is available at: 11583/2704732 since: 2018-04-23T14:23:53Z

Publisher:
IEEE OSA

Published
DOI:10.1364/JOCN.10.000493

Terms of use:

This article is made available under terms and conditions as specified in the corresponding bibliographic description in the repository

Publisher copyright
IEEE postprint/Author's Accepted Manuscript

©2018 IEEE. Personal use of this material is permitted. Permission from IEEE must be obtained for all other uses, in any current or future media, including reprinting/republishing this material for advertising or promotional purposes, creating new collecting works, for resale or lists, or reuse of any copyrighted component of this work in other works.

(Article begins on next page)

17 July 2024

Impact of the Overall Electrical Filter Shaping in Next-Generation 25 and 50 Gb/s PONs

Pablo Torres-Ferrera, Valter Ferrero, Maurizio Valvo, and Roberto Gaudino

***Abstract*—Next-generation high-speed passive optical networks (HS-PONs) supporting 25, 50, and 100 Gb/s are in the early stages of their standardization process. One key aspect under discussion is the choice of the best modulation format for the transceivers. Performance comparisons among several modulation formats against different physical constraints have been presented in literature and are still being examined. In our present contribution, we performed an exhaustive analysis on the impact of the electrical frequency response of transceivers on the performance of two-level pulse amplitude modulation (PAM-2), 4-level PAM (PAM-4), electrical duobinary, and optical duobinary modulation formats with adaptive equalizers on the receiver side. We show, by means of numerical simulations, that the specification of the typically used −3 dB bandwidth is insufficient, since out-of-band electrical frequency response specifications (such as the −20 dB bandwidth) have a huge impact on the performance of the analyzed modulation formats. We believe that the normalized performance graphs given at the end of the paper in terms of −3 dB and −20 dB bandwidths can thus be useful for the design of next-generation HS-PON transceivers.**

***Index Terms*—Adaptive equalization; APD; Duobinary; Filtering; PAM; PON.**

I. Introduction

Standardization efforts to define the physical layer characteristics of next-generation high-speed passive optical networks (HS-PONs) are currently being carried out in the International Telecommunication Union (ITU), Full Service Access Network (FSAN) Group, and the Institute of Electrical and Electronics Engineers (IEEE) standardization bodies [1–5]. Several research analyses are currently ongoing to choose the best modulation format for HS-PON transceivers for different bit rates under consideration (such as 25, 40, and 50 Gb/s) [6–17]. Due to a low cost constraint, particularly for the optical network unit (ONU) (i.e., user) side, several groups are considering if the transmitter and receiver optoelectronics developed for lower bit rates can be re-used for the new higher capacity transceivers when associated to more bandwidth efficient modulation formats and/or adaptive equalization (AEQ). In particular, it would be interesting to re-use the optoelectronics developed for a 10 Gb/s PON for the 25 Gb/s target (and even for the 40 or 50 Gb/s ones), and similarly re-use the 25 Gb/s technology developed for the intra-datacenter short-range transceivers, also for 40–50 Gb/s PONs.

The motivation of this work is thus to analyze the feasibility of these goals, focusing on the fact that these transceivers would be severely electrically band-limited when used for the new target bit rates envisioned for HS-PONs (25 and 50 Gb/s). While previous papers in this area usually only focus on the −3 dB bandwidth [18,19], or experimentally on a single given transceiver, we believe our approach is unique because this paper demonstrates, through extensive analyses, the strong impact of the overall frequency transfer function on system performance. We analyzed traditional intensity-modulation transmitters and direct-detection (DD) receivers followed by a digital signal processing (DSP)-based adaptive equalizer. We show that the *out-of-band* transceiver electrical frequency response is important for the modulation formats under consideration that are PAM-2 (i.e., binary on-off keying), PAM-4, electrical duobinary (EDB) [6,11], and optical duobinary (ODB) [8]. Specifically, we provide normalized graphs showing the joint impact of the −3 dB and −20 dB parameters of the frequency response on the system performance. We believe that these graphs offer a useful contribution to the current discussion in the aforementioned HS-PON standardization bodies and to the transceiver vendors that, depending on the details of their optoelectronic technology, can better select how to optimize their component design.

Thanks to our simulative approach, we were able to span a very large set of parameters (−3 dB bandwidth, −20 dB bandwidth, accumulated dispersion, etc.) and then obtain power penalty curves at a specific bit error rate (BER) value for the four different modulation formats. Moreover, we superimposed on our simulative results the expected bandwidths of several existing transmitters and receivers, thus giving a very broad review of the existing literature in this field.

Summarizing our previous considerations, we believe that the main contribution of this paper is in offering design rules for the transceivers' full electrical frequency

Manuscript received February 2, 2018; revised March 6, 2018; accepted March 6, 2018; published 0, 0000 (Doc. ID 321310).

P. Torres-Ferrera (e-mail: pablo.torres@polito.it), V. Ferrero, and R. Gaudino are with Politecnico di Torino, Dipartimento di Elettronica e Telecomunicazioni, Torino, Italy.

M. Valvo is with Telecom Italia (TIM), Torino, Italy.

https://doi.org/10.1364/JOCN.99.099999

response for different modulation formats. Consequently, our analysis points out the different resiliencies of each modulation format to variations in the available bandwidth and provides information that again can be interesting for component designers. We also report an extensive review of the transfer function of many transmit and receive options (TXs and RXs) presented in the literature, and we give their positioning in our performance estimation graphs.

To this end, the paper is organized in six sections. In Section II, we present the details of the considered transceiver and link architecture and of our simulation environments. In Section III, we discuss different frequency response characteristics, and apply it in Section IV, evaluating the resulting power budget penalty versus filter shape parameters. In Section V, we also introduce the impact of the typical chromatic dispersion accumulated in a PON for different choices of the wavelength band. Finally, we draw a conclusion in Section VI.

II. Simulation Setup

The transceiver and link architecture that we considered in our simulation setup is shown in Fig. 1, where the variable optical attenuator (VOA) is used to span different values of link loss, including the impact of the $1 \times N$ PON splitting ratio. For space limitation, we will not consider the penalty arising from burst mode transmission. Apart from this (important [20]) consideration, our analysis can be applied to both the downstream and upstream directions of a PON link.

At the transmitter side, a binary signal at bit rate R_b (equal to either 25 or 50 Gb/s) is generated by means of a pseudorandom bit sequence (PRBS) $2^{17} - 1$ bits long. The bit stream feeds the electrical TX that creates the appropriate driving signal to generate PAM-2, PAM-4, EDB, or ODB signals in the optical domain. We considered the use of external modulation in this paper or more in general optical transmitters characterized by negligible chirp. The generated electrical signal indicated as $x(t)$ in Fig. 1 is obtained in different ways depending on the modulation format:

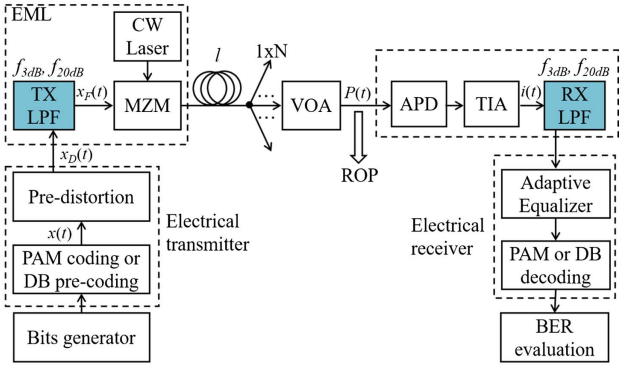

F1:1 Fig. 1. Simulation setup.

(i) In PAM-2 and PAM-4 cases, the binary signal is mapped into a 2-level or 4-level symbol stream, respectively. Gray coding is used in PAM-4.
(ii) In both EDB and ODB cases, the binary signal is digitally pre-coded by applying a standard XOR-based scheme [11]. The resulting 2-level pre-coded signal will eventually turn into a 3-level DB signal thanks to the intrinsic low-pass filtering response of the transceiver. We avoid the use of additional add-and-delay encoding or low-pass electrical filter circuits.

Time-domain simulations are performed using internally developed code fully written in a well-known commercial numerical software. Eight samples per bit (spb) were set. The signal $x(t)$ is normalized to $0 \le x(t) \le 1$. We then assume that the DSP can compensate the Mach-Zehnder modulator (MZM) $\cos^2(\cdot)$ instantaneous nonlinear response by applying the pre-distortion,

$$x_D(t) = \frac{A}{\pi} \arccos(1 - 2x(t)) - V_b, \tag{1}$$

where A is an amplitude factor and V_b is the bias-voltage of the MZM. The pre-distorted signal $x_D(t)$ is then filtered using an electrical low-pass filter (LPF) that emulates the electrical frequency response of the TX. The shape of this filter (and the following one at the RX) is one of the main goals of our investigation. Details on the assumed filter shapes will be given in the Section III. The resulting electrical signal after filtering, $x_F(t)$, drives an optical modulator, optically fed by a continuous wave (CW) electrical field, $E_{\mathrm{CW}}(t)$, generated by the TX laser. The electrical LPF, the optical modulator, and the laser compose the externally modulated laser (EML) block. The optical signal at the output of the EML is modeled using a classical (chirpless) MZM equation,

$$E_{\mathrm{EML}}(t) = E_{\mathrm{CW}}(t) \cos \frac{\pi x_F(t)}{V_\pi}, \tag{2}$$

where V_π is the π-voltage of the modulator. By setting both parameters, A and V_b, of Eq. (1) equal to $V_\pi/2$ for PAM-2, PAM-4, and EDB, or equal to V_π for ODB, the MZM is operated in quadrature or null, respectively. The modulated optical signal is then propagated through a conventional single-mode fiber (SMF). Only chromatic dispersion is considered in the fiber model since the nonlinear effects are assumed to be negligible for the relatively short reach ($\le$20 km) applications and power levels under study. The received optical signal is detected by means of an avalanche photodetector (APD) at the receiver (RX) side followed by a transimpedance amplifier (TIA). The APD + TIA configuration currently seems to be the most likely to be applied for a 40-gigabit-capable PON (NG-PON2) and a 10-gigabit-capable symmetric PON (XGS-PON), which is why we decided to focus on it. The photocurrent that outputs the APD + TIA is evaluated by

$$i(t) = \mathrm{GRP}(t) + n_S(t) + n_T(t), \tag{3}$$

where R is the APD responsivity (assumed to be $R = 0.8$ A/W), G is the APD gain factor [assumed to be $G = 25$ (14 dB)] [21,22], and $P(t)$ is the optical signal instantaneous power that feeds the APD. The signals $n_S(t)$ and $n_T(t)$ emulate the shot noise and thermal noise, respectively. They are modeled as Gaussian random processes with zero-mean and variances given by [23]

$$\sigma_S^2(t) = qG^2\mathrm{FRP}(t)\Delta f_s, \tag{4}$$

$$\sigma_T^2 = N_0\Delta f_s, \tag{5}$$

respectively, where F is the APD excess noise factor (we assumed $F = G^{0.75} = 10.5$ dB), q is the electron charge, N_0 is the input-referred electrical current thermal noise power spectral density ($N_0 = 1.024 \times 10^{-21} A^2/\mathrm{Hz}$), and Δf_s is the bandwidth of the simulation ($\Delta f_s = \mathrm{spb} \cdot R_b$). The overall thermal noise of APD and TIA contributions are included in the $n_T(t)$ noise term. The numerical values assumed here are just indicative values for today's typical 10G PON receivers. Since we present our results in terms of the relative power penalty among different modulation formats (see Sections IV and V), their actual values, however, will have relatively little impact on the penalty graphs.

After the APD + TIA, an electrical LPF emulates the RX frequency response. The characteristics of this RX LPF are the same as the TX LPF, and they are described in the next section. We know that this is not the more general case since the TX and RX filter shapes are independent. We introduce this assumption to limit the number of free parameters to be spanned. In the next section, an extended discussion regarding this consideration is presented.

Since we want to focus on severely band-limited transceivers, we assume that the received electrical signal is equalized by an adaptive feed-forward equalizer (FFE) using least-mean square (LMS) as an adaptation algorithm [19,24] with two samples per symbol and 20 taps. This number of taps was selected to guarantee the right operation of the system in very dispersive and band-limited scenarios. In some cases, however, the system can operate with fewer taps without an additional penalty. The equalizer is trained with a proper pilot sequence, which for PAM-2, PAM-4, and ODB is simply the original transmitted symbol sequence. For EDB, we use a 3-level DB symbol stream obtained after encoding the input pre-coded signal by means of an add-and-delay block. The equalized signal is then decoded according to the employed modulation format. Finally, the bit error rate (BER) is evaluated using direct error counting over 1.3×10^5 bits (after the training sequence), a situation that is very CPU-time demanding, but allows very precise estimation of the BER around the 10^{-3} target value.

The main figure of merit employed in this work to evaluate the performance of the system is the sensitivity (S), defined as the received optical power (ROP) in dBm to reach a BER target of 10^{-3} (i.e, the pre-FEC value selected, for instance, for NG-PON2 in ITU-T G.989.2 for 10 Gb/s).

III. Filtering Considerations

We emulate narrowband transceivers using two electrical LPFs, one at the TX side and one at the RX side. One key parameter of a transceiver frequency response is obviously its –3 dB electrical bandwidth ($f_{3\,\mathrm{dB}}$). Most of the experimental and commercial device characterizations provide information about this parameter. However, as the main target of our work, we focus on the fact that not only the $f_{3\,\mathrm{dB}}$ parameter is fundamental, but the out-of-band (i.e., $f > f_{3\,\mathrm{dB}}$) frequency response of the devices also has a strong impact on the overall system performance. We show, for instance, that for the same $f_{3\,\mathrm{dB}}$ value, very different performance can be achieved depending on the actual value of, say, the –20 dB bandwidth. Moreover, we will show that the sensitivity versus this last parameter is very different, depending on the modulation format used. To the best of our knowledge, this is a novel analysis for the HS-PON scenario, since the out-of-band transceiver electrical frequency characterization is barely ever considered in detail in the available literature. To investigate the relevance of this out-of-band filter shaping, we introduce the –20 dB bandwidth parameter ($f_{20\,\mathrm{dB}}$) in our present analysis. The joint impact of the $f_{3\,\mathrm{dB}}$ and the $f_{20\,\mathrm{dB}}$ parameters is then tested, providing an extra degree of information regarding the impact of the filtering shape on the performance. We present most of our results using the parameters $\mathrm{B}_{3\,\mathrm{dB}}$ and $\mathrm{B}_{20\,\mathrm{dB}}$, which are a representation of $f_{3\,\mathrm{dB}}$ and $f_{20\,\mathrm{dB}}$, respectively, normalized to the bit rate, expressed in percentages, and thus defined as

$$\mathrm{B}_{3\,\mathrm{dB}}[\%] = \frac{f_{3\,\mathrm{dB}}}{R_b} \times 100 \quad \text{and} \quad \mathrm{B}_{20\,\mathrm{dB}}[\%] = \frac{f_{20\,\mathrm{dB}}}{R_b} \times 100. \tag{6}$$

The degrees of freedom in electrical filter shapes are obviously infinite, so we had to make a somewhat arbitrary decision and select a few canonical transfer functions used in the literature [25]. We opted for the Butterworth (BF) and super-Gaussian filter (GF) profiles. Because the former is straightforward, it was selected to exactly set the desired $f_{3\,\mathrm{dB}}$ parameter and to characterize it in terms of the number of poles [25]. Moreover, the BF frequency response is as flat as possible in the passband [25], thus reducing, as compared to other filter types, the in-band shape variations (for a fixed passband bandwidth) when changing the out-of-band steepness. This feature is useful if researchers want to analyze the impact of the out-of-band shape variations as independently as possible on the in-band shape changes (as in the present contribution). However, in BF and for a fixed $f_{3\,\mathrm{dB}}$, the value of the $f_{20\,\mathrm{dB}}$ parameter is subject to the choice of the number of poles of the filter (that is, an integer number) and, consequently, $f_{20\,\mathrm{dB}}$ can be only changed over given (and quite coarse) discrete values. Therefore, for BF, it is not possible to set any arbitrary combination of the $f_{3\,\mathrm{dB}}$ and $f_{20\,\mathrm{dB}}$ parameters. The use of GFs overcomes this limitation by allowing an independent variation of $f_{3\,\mathrm{dB}}$ and $f_{20\,\mathrm{dB}}$. The frequency profile of a GF is defined here as [26]

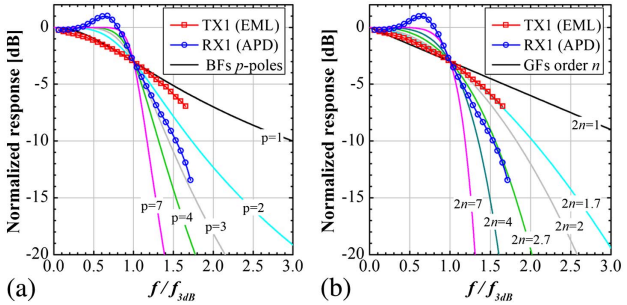

F2:1 Fig. 2. (a) Butterworth (BF) and (b) Super-Gaussian filter (GF)
F2:2 profiles, for different numbers of poles and order, respectively.
F2:3 The normalized experimental response of the TX (EML) and the
F2:4 RX (APD) found in literature [17] are also shown.

$$H(f) = \exp\left(-\frac{1}{2}\left(\frac{f}{f_0}\right)^{2n}\right), \tag{7}$$

where n is the order of the GF filter (which now does not necessarily need to be an integer) and f_0 is a free parameter. The two free and real values, n and f_0, can be set to obtain a frequency response having any possible combination of $f_{3\,\mathrm{dB}}$ and $f_{20\,\mathrm{dB}}$ (as long as $f_{20\,\mathrm{dB}} \geq f_{3\,\mathrm{dB}}$). In Figs. 2(a) and 2(b), the filter shape profiles of the BF and GF models, respectively, are presented for different numbers of poles and order, using on the x-axis as the frequency normalized to $f_{3\,\mathrm{dB}}$. The frequency responses of a realistic TX-RX pair experimentally reported in [17] are also displayed in the figure. From Fig. 2 it can be seen that, after a proper fitting of its two degrees of freedom, the GF model allows a good emulation of the out-of-band frequency response of the realistic TX and RX. The fitting using the BF model is less precise, due to the aforementioned discretization on the number of poles. This result also shows that a realistic transceiver cannot be easily modeled using zeros and poles rationale transfer functions if one must emulate accurately the frequency response also above the 3 dB band. Having said this, most of the results in Sections IV and V will be presented for both GF and BF models to have a full view of the filter shaping problem.

The most significant simplifying assumption made in this work is that the TX and RX LPFs are identical (i.e., they have the same filter shape). Although, this approach may not appear very realistic, a systematic analysis testing different combinations of $f_{3\,\mathrm{dB}}$ and $f_{20\,\mathrm{dB}}$ values in both the TX and RX filters would require studying a huge number of cases and several degrees of freedom, which is very impractical. We found that the equivalent filter formed after cascading any pair of TX and RX identical LPFs can approach well the overall equivalent frequency response formed by any particular combination of real TX and RX devices with different filter shaping (i.e., TX and RX with different $f_{3\,\mathrm{dB}}$ and $f_{20\,\mathrm{dB}}$ values). As a practical example, the same TX-RX pair taken from [17] and already represented in Fig. 2 (TX1 EML $f_{3\,\mathrm{dB}} = 8.9$ GHz, RX1 APD $f_{3\,\mathrm{dB}} = 7.5$ GHz) is used again in Fig. 3 to obtain the concatenated TX + RX transfer function, shown by a solid black curve. On the same figure, the response of the cascade of two identical GFs (or BFs) is shown in dashed green (or dotted pink, for a pair of

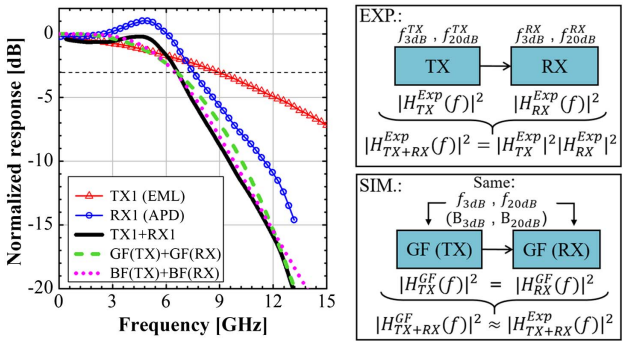

F3:1 Fig. 3. Left side: TX (EML) and RX (APD) frequency characteri-
F3:2 zation reported in [17]. In solid black, the TX+RX equivalent re-
F3:3 sponse. In dashed (dotted), the equivalent frequency response of
F3:4 a pair of identical GFs (BFs), with the same $B_{3\,\mathrm{dB}}$ and $B_{20\,\mathrm{dB}}$.
F3:5 Right side: Diagram of our employed best-fitting procedure
F3:6 (EXP, Experimental data, and SIM, Simulation approach).

identical BFs) curve. In the case of GFs, a good matching with the solid black curve was obtained with two identical GFs, each with $f_{3\,\mathrm{dB}}$ equal to 8.5 GHz and $f_{20\,\mathrm{dB}}$ equal to 17 GHz. The equivalent pair of identical BFs are 2-pole filters, each with $f_{3\,\mathrm{dB}}$ equal to 8.1 GHz.

We followed this fitting procedure (shown in Fig. 3) for a large set of experimental devices reported in the literature. In particular, we evaluated the $f_{3\,\mathrm{dB}}$ and $f_{20\,\mathrm{dB}}$ values (and corresponding $B_{3\,\mathrm{dB}}$ and $B_{20\,\mathrm{dB}}$) of the GFs whose cascaded responses best matched the cascaded response of experimental or commercial TX + RX devices (see Fig. 3, right-hand diagram), and we summarized the results in Table I. Please note that all of these TX and RX devices were developed for standard NRZ 10 Gb/s transmission, which we will label in the rest of the paper as *10G*

TABLE I

NORMALIZED (FOR 25 OR 50 Gb/s TRANSMISSION) –3 dB AND –20 dB BANDWIDTH ($B_{3\,\mathrm{dB}}$ AND $B_{20\,\mathrm{dB}}$) FOR EACH OF THE IDENTICAL GFS AT TX AND RX WHOSE CASCADE RESPONSE BEST FITS THE EQUIVALENT RESPONSE OF THE TX + RX 10G COMPONENTS REPORTED IN THE REFERENCES

	TX (Exp.)		RX (Exp.)		GF, $R_b = 25$		GF, $R_b = 50$	
C.	Ref.	$f^{TX}_{3\,\mathrm{dB}}$	Ref.	$f^{RX}_{3\,\mathrm{dB}}$	$B_{3\,\mathrm{dB}}$	$B_{20\,\mathrm{dB}}$	$B_{3\,\mathrm{dB}}$	$B_{20\,\mathrm{dB}}$
1	[17]	8.9	[17]	7.5	34	68	17	34
2	[17]	8.9	[28]	8.8	32.8	112	16.4	56
3	[17]	8.9	[29]	8.1	32	136	16	68
4	[17]	8.9	[22]	6.8	29.6	96	14.8	48
5	[27]	7.7	[17]	7.5	32	56	16	28
6	[27]	7.7	[28]	8.8	27.6	80	13.8	40
7	[27]	7.7	[29]	8.1	28	96	14	48
8	[27]	7.7	[22]	6.8	26.8	72	13.4	36
9	[a]	9.9	[17]	7.5	34	70	17	35
10	[a]	9.9	[28]	8.8	35.2	100	17.6	50
11	[a]	9.9	[29]	8.1	34.8	128	17.4	64
12	[a]	9.9	[22]	7.5	31.6	92	15.8	46
13	[30][b]: $f^{Sys}_{3\,\mathrm{dB}} = 6.3$ GHz				33.2	70	16.6	35

C.: Case. $f^{TX}_{3\,\mathrm{dB}}$ and $f^{RX}_{3\,\mathrm{dB}}$ in GHz. $B_{3\,\mathrm{dB}}$ and $B_{20\,\mathrm{dB}}$ in %. R_b in Gb/s.
[a]NG-PON2 TX characterization provided by Telecom Italia.
[b]In this particular case, $f^{Sys}_{3\,\mathrm{dB}}$ indicates: $f_{3\,\mathrm{dB}}$ of the overall system.

TABLE II
NORMALIZED (FOR 50 Gb/s TRANSMISSION) −3 dB AND −20 dB BANDWIDTH ($B_{3\,dB}$ AND $B_{20\,dB}$) OF EACH OF THE IDENTICAL GFs AT TX AND RX WHOSE CASCADE RESPONSE BEST FITS THE EQUIVALENT RESPONSE OF THE TX + RX 25G COMPONENTS REPORTED IN THE REFERENCES

	TX (Exp.)		RX (Exp.)		GF, R_b = 50 Gb/s	
C.	Ref.	[GHz]	Ref.	$f_{3\,dB}^{RX}$ [GHz]	$B_{3\,dB}$%	$B_{20\,dB}$%
1	[31]	18.9	[33]	15.8	34	60
2	[31]	18.9	[34]	24.5	40	132
3	[31]	18.9	[35]	32	45	140
4	[31]	18.9	[36]	19.9	40	88
5	[32]	28.2	[33]	15.8	32	58
6	[32]	28.2	[34]	24.5	50	130
7	[32]	28.2	[35]	32	50	110
8	[32]	28.2	[36]	19.9	44	88
9	[27]	23.9	[33]	15.8	30	58
10	[27]	23.9	[34]	24.5	42	84
11	[27]	23.9	[35]	32	44	90
12	[27]	23.9	[36]	19.9	38	78

technology. In Table II, the same information is reported for another set of experimental devices reported in literature for the 25 Gb/s transmission, called in this paper 25G technology. The information provided in Tables I and II is very helpful to contextualize our results in the framework of state-of-the-art technology.

From Table I, we can observe that the same couple of TX-RX devices has associated with a different pair of $B_{3\,dB}$ and $B_{20\,dB}$, depending on the value of R_b. This arises because, although the $f_{3\,dB}$ and $f_{20\,dB}$ parameters of the corresponding identical GFs are the same irrespective of R_b, the $B_{3\,dB}$ and $B_{20\,dB}$ values are normalized to the bit rate, as indicated in Eq. (6).

IV. BACK-TO-BACK RESULTS

A back-to-back (BtB) performance comparison among the four modulation formats is presented in this section. For BtB, we mean a simulation that emulates the transceiver bandwidth limitations (thus taking into account only the filtering effects in the TX and RX), the electro-optical and opto-electrical conversions, and the noise at the receiver. The effect of the fiber (i.e., chromatic dispersion) will then be introduced in the next section.

We started the BtB analysis by considering 1-pole BFs as the electrical frequency response of each TX and RX device. In the inset of Fig. 4(a), we report the filter profiles of the individual TX, or RX, 1-pole BF (solid) and the cascaded response of them (dotted), for a (single filter) $f_{3\,dB}$ = 7 GHz. To enable a fair comparison, the performance is evaluated in terms of the power penalty taking as a reference the sensitivity of PAM-2 in its optimal conditions (without any BW limitations and in a BtB scenario). This sensitivity (the ROP to guarantee 10^{-3} BER) is termed S_0, and, for the APD noise levels reported in the previous section, it is equal to S_0 = −28.1 dBm for R_b = 25 Gb/s, and S_0 = −25.7 dBm for R_b = 50 Gb/s. The computed power penalty

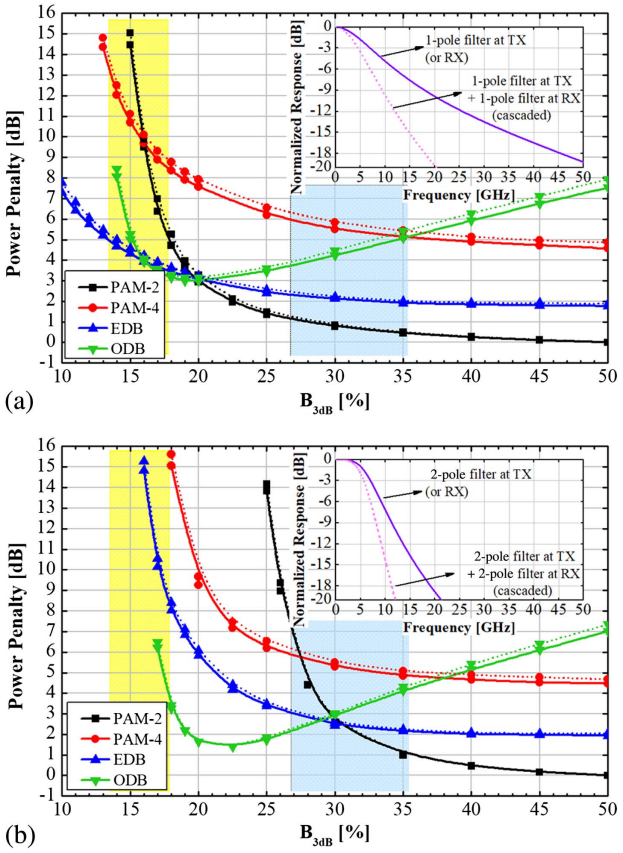

Fig. 4. Performance comparison among modulation formats in terms of the power penalty with respect to S_0, the PAM-2 sensitivity in the best condition (BtB unlimited bandwidth case, S_0 = −28.1 dBm for 25 Gb/s and S_0 = −25.7 dBm for 50 Gb/s), as a function of the $B_{3\,dB}$ of the filters. (a) 1-pole BF and (b) 2-pole BF (depicted in the inset). Solid lines for R_b = 25 Gb/s, dotted lines for R_b = 50 Gb/s. Colored regions: In blue (yellow): 10G technology to transmit 25 (50) Gb/s.

of each modulation format as a function of the $B_{3\,dB}$ parameter is shown in Fig. 4(a), for both analyzed bit rates: 25 Gb/s (solid) and 50 Gb/s (dotted). Thanks to the employed definition of the power penalty, there is a very close match between the results of the two analyzed bit rates, as demonstrated by the fact that the difference between the solid (25 Gb/s) and dotted (50 Gb/s) curves is negligible irrespective of the modulation format. By using the information provided in Table I, we also superimposed on Fig. 4 a pair of colored regions that qualitatively indicate the range of $B_{3\,dB}$ values that current 10G technology transceivers exhibit when transmitting at 25 Gb/s (in blue) and 50 Gb/s (in yellow).

From Fig. 4 we can observe that in spite of using AEQ, the impact of limited system bandwidths is not completely canceled (as expected for an FFE-LMS-based AEQ [24] operating over a noisy signal). However, we have verified that the penalty due to system bandwidth reduction is much less pronounced using the AEQ scenario considered in this paper than for a not-equalized receiver (we cannot show the relative comparison here due to space limitations).

As discussed in the previous section, a 1-pole filter is very likely too optimistic for most realistic transceivers. To explore the impact of the out-of-band filter shaping on the analyzed modulation formats performance, the procedure to obtain the results presented in Fig. 4(a) is performed again using 2-pole BFs, but keeping the other assumptions the same. The corresponding results obtained under this new situation are presented in Fig. 4(b). One of the key points of our paper can be seen here: The out-of-band steepness of the transceivers' frequency response significantly affects the system performance even for the same –3 dB bandwidth, and changes the performance ranking of the different modulation formats. For instance, let us consider the transmission of 25 Gb/s using 10G technology-based transceivers (case referred here as 25G/10G, shown in the blue-colored area of Fig. 4). In this situation, if the transceiver response is modeled using a 1-pole BF approach, PAM-2 outperforms the rest of the modulation formats in the complete 25G/10G (blue) region. However, if the filter's response model changes from one- to two-pole BF [Fig. 4(b)] PAM-2 starts to become critical, and it is, for instance, surpassed by EDB in part of the 25G/10G region of the graph. As another example, let us now consider the transmission of 50 Gb/s using 10G technology (case referred to here as 50G/10G, shown in the yellow colored area of Fig. 4). From Fig. 4(a), we can observe that EDB, ODB, and even PAM-4 (with a strong penalty) could be feasible alternatives for the 50G/10G transmission if a 1-pole filter case is considered (while PAM-2 is clearly out of the question). If we again change the filter response to a 2-pole profile, we can see from Fig. 4(b) that even EDB, ODB, or PAM-4 would operate in a region with exceedingly high penalty.

These first two examples show the performance dependency of the modulation formats versus the transceivers' frequency response, not only in terms of the –3 dB bandwidth (as commonly done in much of the analysis in the current literature), but also as a function of the out-of-band (i.e., above the –3 dB point) filter steepness.

We thus prosecute our analysis by also considering a parameter that would characterize the out-of-band response. As mentioned in Section III, we selected for this goal the frequency at a –20 dB attenuation (i.e., the $f_{20\,\mathrm{dB}}$ parameter and its normalized version, $B_{20\,\mathrm{dB}}$). Note that another reference attenuation value could also have been chosen to quantify the degree of tilting of the out-of-band response. The use of the –20 dB attenuation value was selected arbitrarily but, as we will show, it turned out to be a very relevant parameter.

To start the out-of-band filter impact analysis, we fixed the $B_{3\,\mathrm{dB}}$ parameter to 28%, which is a representative state-of-the art case for the 25G/10G transmission as shown in Table I, and varied the number of poles of the BFs. As shown in Fig. 2(a), for a BF with a given $f_{3\,\mathrm{dB}}$, increasing the number of poles corresponds to an increase in the out-of-band filter steepness, and a decrease in its –20 dB bandwidth. The performance of the four modulation formats in terms of the relative power penalty as a function of the BF number of poles (or the corresponding $B_{20\,\mathrm{dB}}$ parameter) is shown in Fig. 5 (markers only), for 25 Gb/s transmission.

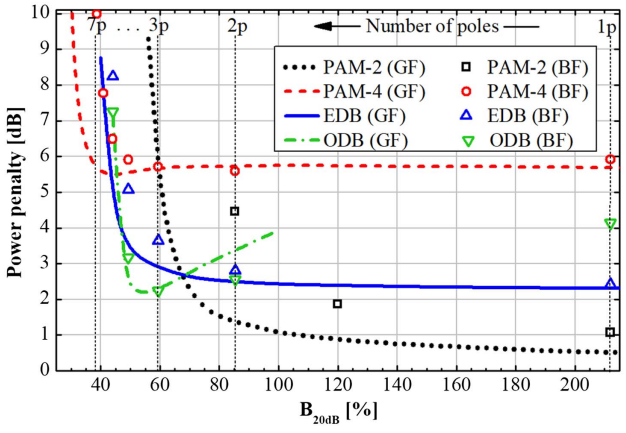

Fig. 5. Performance comparison in terms of $B_{20\,\mathrm{dB}}$ using BF (only marker curves) and GF (only line curves). A 25 Gb/s transmission is considered. The $B_{3\,\mathrm{dB}}$ is fixed to 28% ($f_{3\,\mathrm{dB}} = 7$ GHz for $R_b = 25$ Gb/s). The power penalty is relative to PAM-2 $S_0 = -28.1$ dBm for $R_b = 25$ Gb/s. F5:1 F5:2 F5:3 F5:4 F5:5

Since the number of poles is an integer parameter, only certain discrete $B_{20\,\mathrm{dB}}$ values can be evaluated. To overcome this too coarse discretization of $B_{20\,\mathrm{dB}}$, the use of the GF model to emulate the transceiver frequency response is introduced. Under this GF approach, continuous curves of a relative power penalty versus $B_{20\,\mathrm{dB}}$ can now be obtained, and are depicted in Fig. 5 (curves without markers). Apart from the differences that occur using the BF or GF model, Fig. 5 shows with evidence the great relevance of the exact value of the out-of-band filter shape and, again, the fact that the performance ranking among modulation formats is also greatly affected by this parameter. For instance, although PAM-2 is the best modulation format in the $B_{20\,\mathrm{dB}} > 120\%$ region, for $B_{20\,\mathrm{dB}} \leq 70\%$ PAM-2 starts to become exceedingly critical in terms of the penalty. The EDB solution has, on the contrary, a good resilience for low $B_{20\,\mathrm{dB}}$ values, showing just small penalties down to the $B_{20\,\mathrm{dB}} = 50\%$ region. PAM-4 also exhibits a good tolerance, even for $B_{20\,\mathrm{dB}} = 40\%$. ODB has a very peculiar behavior, showing both in Fig. 4 (versus $B_{3\,\mathrm{dB}}$) and Fig. 5 (versus $B_{20\,\mathrm{dB}}$) that it may be considered the best modulation format for very low bandwidths, but only if the $B_{3\,\mathrm{dB}}$ and $B_{20\,\mathrm{dB}}$ are optimized to their proper values. However, for $B_{20\,\mathrm{dB}} > 60\%$ values, the ODB sensitivity starts to get worse. The increased penalty shown with the GF approach is attributed to the reduced in-band power that this filter collects with respect to BFs for higher values of $B_{20\,\mathrm{dB}}$ (see Fig. 2). In the case of PAM-2, a close match between the BF and GF filter shape is only found when the filter steepness is very low (around the 1-pole BF case). Please note that for PAM-2, a point between the 1- and 2-pole cases was plotted. This point was measured by setting a 1-pole filter at the TX and a 2-pole filter at the RX (which corresponds to a 3-pole filter when the TX and RX filters are cascaded, emulating symmetric 1.5-poles at the TX and RX situation). This is the only exceptional point that was evaluated using different characteristics at TX and RX filters in this contribution. However, following the same approach, the performance of the system using a 1-pole filter at the TX and a 3-pole filter

at the RX was also tested for PAM-2 (corresponding to a 4-pole filter when cascading the TX and RX, equivalent of having a 2-pole filter at the TX and one at the RX if a linear system is assumed). The sensitivity measured under this situation was the same as having 2-pole filters at TX and RX, which shows that the system behavior is mostly linear, and the cascaded assumptions described in Section III can be considered accurate.

To summarize, Fig. 5 suggests that when ranking the modulation format tolerance against the variation of the $B_{20\,dB}$ parameter, PAM-4 and EDB show the best degree of resilience, PAM-4 being the most robust format for extremely low $B_{20\,dB}$, but obviously starting from its intrinsic penalty that is present compared to PAM-2 for high bandwidths. ODB has very interesting performance, but only for an optimized filter bandwidth, while EDB shows a very good compromise on a very large range of $B_{20\,dB}$ values.

Compared to the actual data extrapolated from commercial transceivers and reported in the aforementioned Tables I and II, we can see that the $B_{20\,dB}$ parameter can vary from around 60% to even 140%, for different state-of-the-art devices. This fact highlights the need to consider the robustness of a modulation format against both in-band and out-of-band filter shaping variations as a relevant parameter.

The results shown in Fig. 5 were obtained for a fixed value of $B_{3\,dB} = 28\%$. For different $B_{3\,dB}$ values, the conclusions may change. We thus performed an extensive study on the impact of a joint variation of the $B_{3\,dB}$ and $B_{20\,dB}$ parameters. Results are presented in Fig. 6, which shows the power penalty of PAM-2 with respect to its best sensitivity S_0 ($S_0 = -28.1$ dBm for $R_b = 25$ Gb/s, and $S_0 = -25.6$ dBm for $R_b = 50$ Gb/s) as a function of both $B_{3\,dB}$ and $B_{20\,dB}$ variables. We believe this is one of the key results of our paper, giving transceiver designers an overview of the best system solutions. Using this graph, a component designer can trade off the component parameters that most affect the $B_{3\,dB}$ and $B_{20\,dB}$, and use the best design choices.

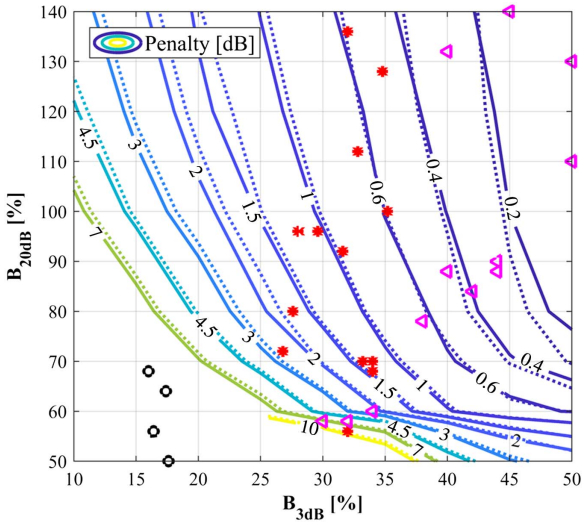

F6:1 Fig. 6. PAM-2 power penalty with respect to the S obtained for
F6:2 PAM-2 in the best condition (BtB unlimited bandwidth case, $S_0 =$
F6:3 -28.1 dBm for 25 Gb/s and $S_0 = -25.7$ dBm for 50 Gb/s) as a
F6:4 function of the GFs $B_{3\,dB}$ and $B_{20\,dB}$ parameters. Red points:
F6:5 25 Gb/s using 10G technology transceivers. Black circles:
F6:6 50 Gb/s using 10G technology transceivers. Pink triangles:
F6:7 50 Gb/s using 25G technology transceivers.

In Fig. 6, the contour plots in solid lines correspond to the 25 Gb/s case, while the ones in dotted lines to the 50 Gb/s transmission. A very good agreement between the solid and dotted curves is again found. Tables I and II show the real frequency response characteristics of the transceivers, which are also displayed in Fig. 6, in which any pair of $B_{3\,dB}$ and $B_{20\,dB}$ is considered as the coordinates of a point in the plane (indicating the operation regions of the current devices). Note the huge transceiver filter shaping impact on the performance. For instance, when using 25G transceivers for 50 Gb/s transmission (pink triangles), considering different real devices we can have a negligible penalty (lower than 0.2 dB in some cases), but in other cases the penalty can reach 10 dB. The same information is plotted in Fig. 7 for the other modulation formats, always evaluating the power penalty with respect to the same PAM-2 S_0 sensitivity values of Fig. 6. Since the same good agreement between the 25 and 50 Gb/s results found for PAM-2 was also corroborated for the other modulation formats, only 50 Gb/s curves (representing both bit rate situations) are shown.

By summarizing all the information provided by Figs. 4–7, we can state the following conclusions with respect to the filter shape impact on the performance of the four different modulation formats in the BtB situation. Let us start by considering the options to transmit 25 Gb/s using 10G technology transceivers (25G/10G):

- PAM-4 exhibits the best tolerance against filter shaping variations, in the sense that its penalty curve versus the reduction in filter bandwidth (for both $B_{3\,dB}$ and $B_{20\,dB}$) remains flat down to very low values. However, this format has a bigger penalty compared to EDB or ODB in the 25G/10G region [see the red points of Figs. 7(a)–7(c), and their associated power penalty].
- ODB exhibits large variations as a function of the $B_{3\,dB}$ and $B_{20\,dB}$ parameter. In the search for low transceiver bandwidth solutions, it has a very interesting behavior, but only around its optimal values. Moreover, it should be remembered that this is the only format that necessarily requires an external modulator (while all the other three modulation formats also can be implemented with directly modulated lasers).
- PAM-2 presents a strong filtering-dependent performance (see Fig. 6). For instance, by using two transceivers having the same $B_{3\,dB} = 30\%$ but very different steepness (i.e., $B_{20\,dB} = 60\%$ and 120%, which is not far from a real situation, as shown by the red points in Fig. 6), a very different penalty of >7 dB versus ~1 dB, respectively, can be obtained. Therefore, PAM-2 is a good alternative only if large bandwidth transceivers are used.

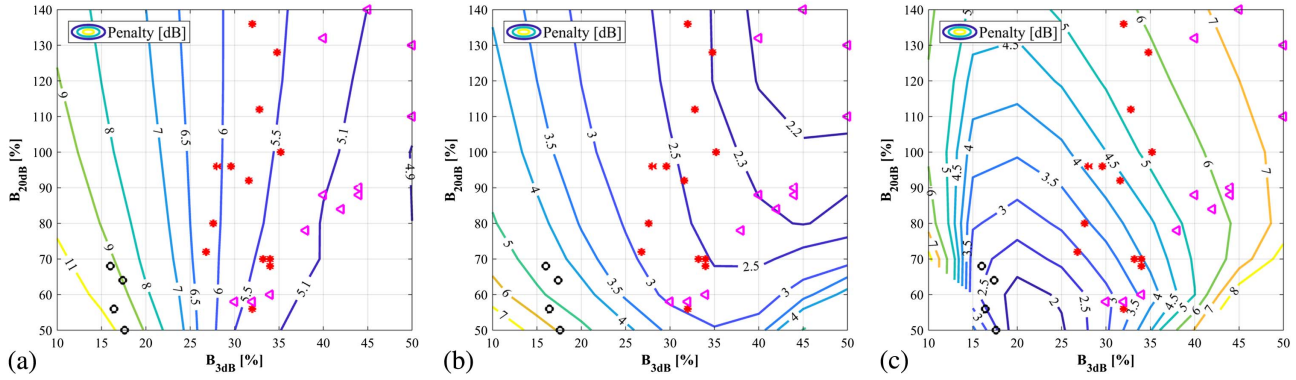

F7:1 Fig. 7. (a) PAM-4, (b) EDB, and (c) ODB power penalty with respect to the S obtained for PAM-2 in the BtB unlimited bandwidth case, $\underline{S_0}$
F7:2 ($\underline{S_0} = -28.1$ dBm for 25 Gb/s and $\underline{S_0} = -25.7$ dBm for 50 Gb/s) as a function of $B_{3\,dB}$ and $B_{20\,dB}$ of the GFs. Red points: 25 Gb/s using 10G
F7:3 technology. Black circles: 50 Gb/s using 10G technology. Pink triangles: 50 Gb/s using 25G technology.

– EDB shows a good tolerance against filtering, and a penalty between 2 and 3 dB in all the cases reported in Table I. Accordingly, EDB seems to be a very interesting alternative in terms of resilience against filtering variations (with respect to both −3 dB bandwidth and steepness).

Let us now consider the option of transmitting 50 Gb/s using 10G technology (50G/10G):

– PAM-2 is not feasible (see the black circles of Fig. 6).
– Neither PAM-4 or EDB seem to be feasible alternatives, since a large power penalty is achieved in this situation [see the black circles of Figs. 7(a) and 7(b)].
– The only modulation format that may be used is ODB [see the black circles of Fig. 7(c)]. However, in the $B_{3\,dB} <$ 15% range, the penalty of ODB rapidly increases even with small −3 dB bandwidth decreases. Therefore, the performance stability can be critical.

Finally, let us consider transmitting 50 Gb/s using 25G technology (50G/25G):

– For PAM-2 and EDB, the same conclusions as in the case of 25G/10G can be extrapolated. However, most 25G technology has more relaxed bandwidth limitations to transmit 50 Gb/s (see pink triangles in Fig. 6). PAM-2 then seems to be a good alternative to transmit 50G/25G. EDB only outperforms it if transceivers with very strong bandwidth limitations are employed.
– PAM-4 and ODB are not good candidates since a large power penalty (>3 dB) arises in this situation.

V. Dispersion Analysis

In Section IV, the effect of the transceivers' filtering characteristics on the performance of four IM/DD modulation formats in a BtB scenario was analyzed. In this section, the previous analysis is extended by also considering the presence of chromatic dispersion in the link.

As a first approach, the $B_{3\,dB}$ and $B_{20\,dB}$ parameters are fixed to some of the values discussed in the previous section and the total dispersion of the link is varied to compute the relative power penalty of the four modulation formats as a function of this last parameter. For the 25 Gb/s transmission, two representative $\{B_{3\,dB}, B_{20\,dB}\}$ pairs were selected: $P1 = \{32\%, 136\%\}$ and $P2 = \{32\%, 56\%\}$ (cases 5 and 3 of Table I, respectively), to compare the power penalty versus dispersion curves obtained when the −3 dB bandwidth of the filters is the same, but the steepness is abruptly changed. The results are displayed in Fig. 8(a). For the 50 Gb/s situation, the following $\{B_{3\,dB}, B_{20\,dB}\}$ pairs were employed: $P3 = \{32\%, 132\%\}$ and $P4 = \{32\%, 58\%\}$ (case 5 of Table II). The corresponding results are shown in Fig. 8(b).

From Fig. 8(a) ($R_b = 25$ Gb/s), we can observe that PAM-4 is the most robust format against the effect of both dispersion and filtering. EDB also exhibits good tolerance against dispersion. We now introduce some practical consideration focusing on the PON scenario, which requires using SMF fibers up to $l = 20$ km in different wavelength bands, which we have grouped as O-band (about 1300 nm, where at the limit of the bandwidth specified by different PON standards the accumulated dispersion can go up to ~100 ps/nm), C-band (1550 nm, accumulated dispersion up to 360 ps/nm), and L-band (1580 nm, up to ~460 ps/nm). Comparing the different modulation

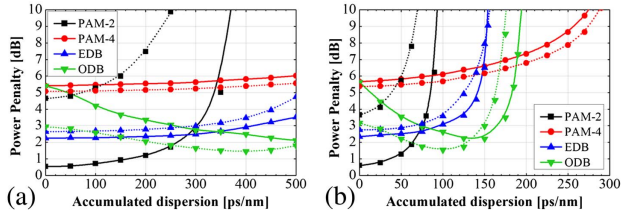

F8:1 Fig. 8. Performance comparison among the four modulation formats in terms of the *relative power penalty* as a function
F8:2 of dispersion. (a) $R_b = 25$ Gb/s; solid: $B_{3\,dB} = 32\%$ and $B_{20\,dB} =$
F8:3 136%; dotted: $B_{3\,dB} = 32\%$ and $B_{20\,dB} = 56\%$; (b) $R_b = 50$ Gb/s;
F8:4 solid: $B_{3\,dB} = 32\%$ and $B_{20\,dB} = 132\%$; dotted: $B_{3\,dB} = 32$ GHz
F8:5 and $B_{20\,dB} = 58\%$. The power penalty is relative to PAM-2 S_0
F8:6 ($S_0 = -28.1$ dBm for $R_b = 25$ Gb/s and $S_0 = -25.7$ dBm for
F8:7 $R_b = 50$ Gb/s).
F8:8

formats, EDB outperforms PAM-4 in O, C, and L optical bands. Regarding PAM-2, as in BtB, in presence of dispersion its performance is also highly affected by the steepness of the out-of-band transceivers' response. Its use in C- or L-band is not feasible for $l = 20$ km. In O-band, its use seems to be strongly constrained to the use of technology with low steepness filtering characteristics. Under these conditions, its performance is the best among all modulation formats. ODB, on the other hand, is the only format in which the performance improves as both the dispersion and steepness of the filters increase (at least in O, C, and L bands with $l = 20$ km). In O-band, ODB is outperformed by EDB, while in the C- and L-bands it seems to be the best alternative.

Regarding the 50 Gb/s transmission [see Fig. 8(b)] over 20 km of fiber, we observed that no modulation format can be used to operate the system in the C-band or L-band. PAM-2 does not work even in the O-band. The only feasible modulation formats (in O-band, $l = 20$ km) are EDB, ODB, and PAM-4, being the performance of PAM-4 surpassed by that of both EDB and ODB in the whole O-band.

Although PAM-4 has been found to be the most resilient format against dispersion and bandwidth limitations in all the analyzed conditions, due to its higher intrinsic penalty as compared to EDB in all the practical scenarios, we do not consider it a feasible alternative for the implementation of 25 Gb/s or 50 Gb/s PON systems over 20 km of fiber. Therefore, we do not analyze this modulation format in the rest of this section. A similar consideration has been performed with respect to PAM-2 operating in the C-band with $R_b = 25$ Gb/s, and the O-band with $R_b = 50$ Gb/s. Therefore, other than the 25 Gb/s O-band case in which PAM-2 can still be considered a feasible format, the rest of this section will be focused on the comparison between EDB and ODB formats.

Some preliminary results allow us to forecast the feasibility of PAM-2 and PAM-4 using pre-chirping in the transmission of 50 Gb/s in the O-band and C-band ($l = 20$ km), respectively, at least under relaxed bandwidth limitations (1-pole BFs case). However, these alternatives need to be further explored under more strict filtering conditions, which is an analysis out of the scope of the present contribution.

We now proceed with some further insight, focusing on 25 Gb/s transmission results. In Figs. 9 and 10 we show, for the O-band and the C-band operation over 20-km of fiber, respectively, the contour plots of the power penalty as a function of $B_{3\,dB}$ and $B_{20\,dB}$, for different modulation formats and for different accumulated dispersion (using the previously indicated notation of the O- and the C-band at 20 km). The power penalty is evaluated in all cases with respect to S_0 of PAM-2 in BtB conditions ($S_0 = -28.1$ dBm for $R_b = 25$ Gb/s).

Regarding O-band operation (Fig. 9), the three modulation formats exhibit similar results to the BtB situation (see Figs. 6 and 7), but have a small dispersion penalty for PAM-2 and EDB. In contrast, ODB exhibits a performance improvement thanks to dispersion, which is consistent with the results presented in Fig. 8. The power penalty of EDB varies between 2.2 and 3 dB when using state-of-the-art transceivers with different −3 dB bandwidth and out-of-band filtering steepness. In contrast, in the case of PAM-2, this penalty can vary from around 0.6 to an exceedingly large value around 10 dB. ODB is an intermediate case (the penalty varies from 2.5 to 4.5 dB). Therefore, we consider EDB as the best alternative for 25 Gb/s 20-km O-band operation with respect to tolerance against frequency response variations. However, PAM-2 can be a good solution; its penalty can be as low as <1 dB, which is a value not achievable by any other format, if *and only if* technology with proper filtering characteristics ($B_{3\,dB} \geq 30\%$ and $B_{20\,dB} \geq 70\%$) can be guaranteed.

When considering C-band operation, we can see from the contour plots shown in Figs. 10(a) and 10(b), that the performance of ODB is further improved by dispersion while the opposite occurs for EDB. This situation tips the scales in favor of ODB in terms of a lower range of power penalty achievable using state-of-the-art devices (i.e., from 1 to 3 dB, in contrast to 2.5 to 3.5 dB achieved with EDB). EDB remains the format with less performance variations as a function of filtering. It is important to note that, by using ODB and small band-limited transceivers

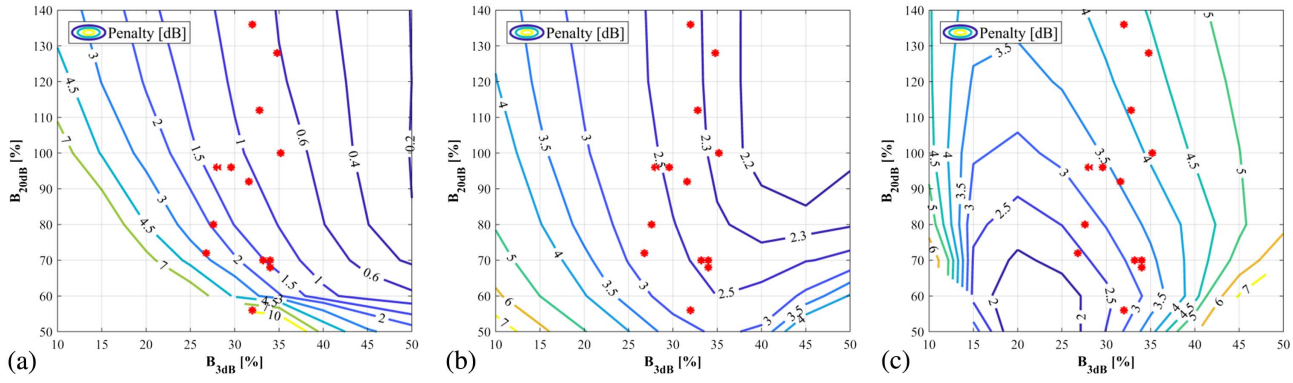

Fig. 9. (a) PAM-2, (b) EDB, and (c) ODB power penalty with respect to the S obtained for PAM-2 in the BtB unlimited bandwidth case, S_0 ($S_0 = -28.1$ dBm) as a function of $B_{3\,dB}$ and $B_{20\,dB}$ of the GFs, for a 25 Gb/s20 km O-band operation. Red points: 25 Gb/s using 10G technology.

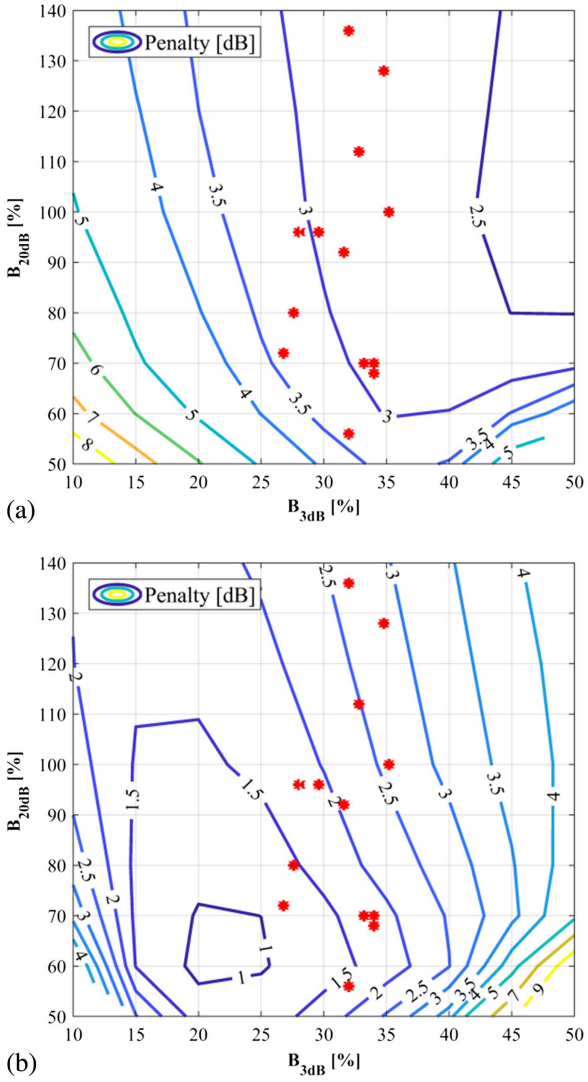

F10:1 Fig. 10. (a) EDB and (b) ODB power penalty with respect to the S
F10:2 obtained for PAM-2 in the BtB unlimited bandwidth case, S_0
F10:3 ($S_0 = -28.1$ dBm) as a function of $B_{3\,dB}$ and $B_{20\,dB}$ of the GFs,
F10:4 for a 25 Gb/s20 km C-band operation. Red points: 25 Gb/s using
F10:5 10G technology.

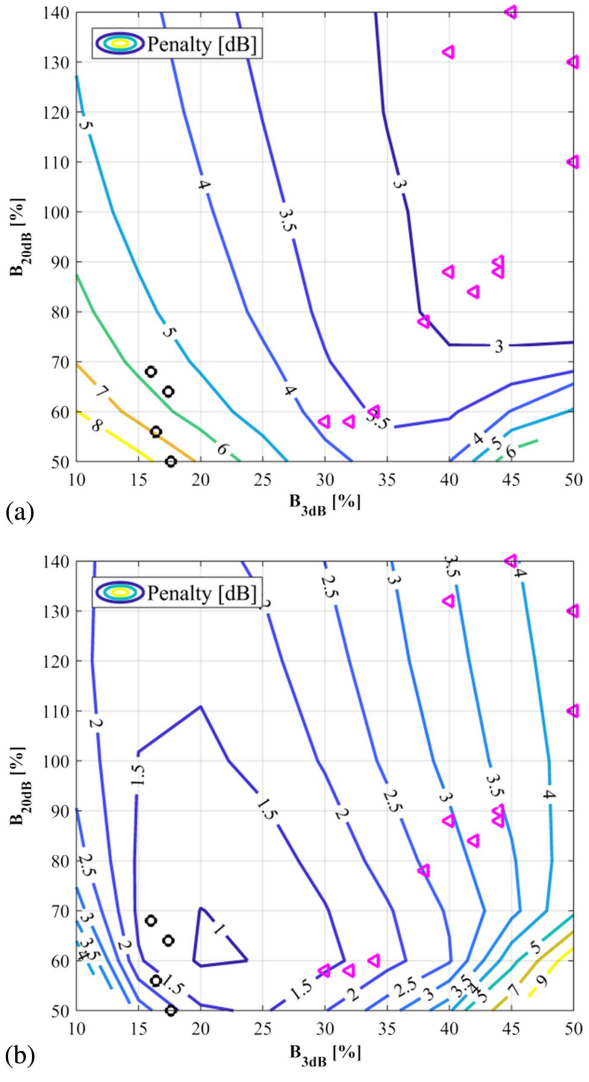

F11:1 Fig. 11. (a) EDB and (b) ODB power penalty with respect to the S
F11:2 obtained for PAM-2 in the BtB unlimited bandwidth case, S_0
F11:3 ($S_0 = -25.6$ dBm) as a function of $B_{3\,dB}$ and $B_{20\,dB}$ of the GFs,
F11:4 for a 50 Gb/s 20 km O-band operation. Black circles: 50 Gb/s us-
F11:5 ing 10G technology. Pink triangles: 50 Gb/s using 25G technology.

727 (i.e., $B_{3\,dB} \geq 35\%$ and $B_{20\,dB} \geq 100\%$), it is always possible to
728 increase the performance of the system by intentionally
729 adding an electrical filter at the TX or RX, to enforce a
730 stronger band-limited condition [close to the optimum
731 point that can be seen in Fig. 10(b)] in which the achievable
732 penalty could be only 1 dB. This feature is not achievable
733 using any other modulation format. Another positive
734 (and unique) feature of ODB is that, as can be seen in Fig. 8,
735 the dispersion penalty decreases as the accumulated
736 dispersion increases (i.e., length), which can compensate,
737 to some degree, for the increase of fiber attenuation as
738 the fiber length augments. In favor of EDB is the fact that
739 it can be implemented with both direct modulation and
740 external modulation (using electro-absorption modulators
741 or a MZM) approaches, while ODB must use a MZM.

742 Let us finally comment on the 50 Gb/s transmission re-
743 sults. In Fig. 11, contour plots of the power penalty as a
744 function of $B_{3\,dB}$ and $B_{20\,dB}$ for 50 Gb/s 20-km O-band op-
745 eration using EDB [Fig. 11(a)] or ODB [Fig. 11(b)], are
746 shown. The power penalty is referred to the 50 Gb/s
747 PAM-2 $S_0 = -25.6$ dBm. The contour plots displayed in
748 Fig. 11 are very similar to those shown in Fig. 10 (for
749 25 Gb/s transmission in 20-km O-band). However, the re-
750 gions of operation of 50G/10G and 50G/25G state-of-the-art
751 devices (see the black circles and pink triangles of Fig. 11,
752 respectively) are different from those of 25G/10G (see the
753 red points of Fig. 10). Therefore, the conclusions between
754 these cases may differ. First, ODB appears to be the only
755 feasible format to transmit 50 Gb/s using 10G technology
756 in O-band. In the black circles of Fig. 11, only the cases 2, 3,
757 10, and 11 in Table I are plotted. The rest of the cases have
758 a $B_{20\,dB} < 50\%$, which corresponds to power penalties
759 higher than 2.5 dB [not shown in Fig. 11(b)]. Then, for

correct operation, the $B_{20\,dB}$ of the TX and RX should at least be higher than 50%.

Regarding the transmission of 50 Gb/s using 25G technology, the maximum penalty achievable with EDB [pink triangles in Fig. 11(a)] and ODB [pink triangles in Fig. 11(b)] is similar (around 4 dB). Again, EDB exhibits a more stable penalty, varying between 3 and 4 dB (mostly around 3 dB), while ODB penalty variation is wider, varying from 1.5 to 4 dB. In terms of tolerance against filtering, we should opt for EDB. However, as mentioned before, with the right technology characteristics or by enforcing the frequency response using an additional electrical filter, we could operate close to the optimal point of ODB and achieve a penalty as low as 1 dB.

VI. Conclusions

In this contribution, we have demonstrated the strong impact on system performance that the overall filter shaping electrical response of the transceivers has on the transmission of 25 and 50 Gb/s using currently available 10 and 25 Gb/s technology and adaptive equalization. Using numerical simulations, we compared the achievable performance of PAM-2, PAM-4, EDB, and ODB under different band-limited and dispersive conditions. We introduced the −20 dB bandwidth parameter to quantify the impact of the out-of-band steepness of the transceivers' response. We demonstrated that this parameter is as relevant as the −3 dB bandwidth when comparing the performance of different modulation formats.

We found that PAM-2 is the best performing format for the transmission of 25 Gb/s using 10G technology in the 20 km O-band, but only if transceivers with relatively small bandwidth limitations can be used. Otherwise, the best alternative is EDB because it is more resilient to filter shaping variations than PAM-2 and outperforms the rest of the formats in terms of penalty.

On the transmission of 25 Gb/s using 10G technology in 20-km C-band, EDB exhibits a slightly higher maximum power penalty than ODB (4 dB versus 3.5 dB). The minimum achievable power penalty of ODB is 1.5 dB lower than that of EDB. However, the performance of EDB as a function of the −3 dB and −20 dB bandwidth is more stable (power penalty variations are less than 1 dB) than in the case of ODB, which has power penalty variations up to 2 dB.

Regarding the 50 Gb/s case, no modulation format works under 20 km of C-band operation. PAM-2 is not even feasible in the O-band. ODB is the only format that can be used if using 10G technology (in the 20 km O-band), but only if some filtering conditions can be guaranteed. If 25G technology is used and the O-band is considered through 20 km of fiber, both EDB and ODB can work, exhibiting a maximum penalty of 4 dB. Again, the penalty of ODB is the minimum under some filtering conditions, but EDB performance is more robust against the filter shaping variations of the transceivers' frequency response.

In all cases, PAM-4 is the most robust format against both dispersion and filtering conditions. However, due to its inherent higher power penalty with respect to the rest of the formats, PAM-4 is always outperformed by any of them in most of the analyzed conditions.

The results presented in this contribution were obtained using identical filters to emulate the frequency response of both the TX and RX. For space limitations, we did not consider more general assumptions and degrees of freedom in our present analysis. Using filters with different characteristics at the TX and RX side, which could give rise to interesting results, is a topic we are currently researching.

Acknowledgment

This work was supported by Telecom Italia under the grant 5G-PON (2017). This work was carried out under the PhotoNext initiative at Politecnico di Torino (http://www.photonext.polito.it/).

References

[1] IEEE P802.3ca 100G-EPON Task Force, "Physical layer specifications and management parameters for 25 Gb/s, 50 Gb/s, and 100 Gb/s passive optical networks," 2015 [Online]. Available: http://www.ieee802.org/3/ca/index.shtml.

[2] Full Service Access Network (FSAN), "Roadmap," 2016 [Online]. Available: https://www.fsan.org/roadmap/.

[3] ITU-T Study Group 15: Networks, "Technologies and infrastructures for transport, access and home," 2017 [Online]. Available: https://www.itu.int/en/ITU-T/studygroups/2017-2020/15/Pages/default.aspx.

[4] V. Houtsma, D. van Veen, and E. Harstead, "Recent progress on standardization of next-generation 25, 50, and 100G EPON," *J. Lightwave Technol.*, vol. 35, no. 6, pp. 1228–1234, 2017.

[5] D. Nesset, "PON roadmap [Invited]," *J. Opt. Commun. Netw.*, vol. 9, pp. A71–A76, 2017.

[6] D. van Veen, V. E. Houtsma, P. Winzer, and P. Vetter, "26-Gbps PON transmission over 40-km using duobinary detection with a low cost 7-GHz APD-based receiver," in *European Conf. Optical Communication (ECOC)*, Amsterdam, The Netherlands, 2012.

[7] Z. Li, L. Yi, X. Wang, and W. Hu, "28 Gb/s duobinary signal transmission over 40 km based on 10 GHz DML and PIN for 100 Gb/s PON," *Opt. Express*, vol. 23, pp. 20249–20256, 2015.

[8] D. van Veen, V. Houtsma, A. H. Gnauck, and P. Iannone, "Demonstration of 40-Gb/s TDM-PON over 42-km with 31 dB optical power budget using an APD-based receiver," *J. Lightwave Technol.*, vol. 33, no. 8, pp. 1675–1680, 2015.

[9] J. Wei, N. Eiselt, H. Griesser, K. Grobe, M. H. Eiselt, J. J. V. Olmos, I. T. Monroy, and J.-P. Elbers, "Demonstration of the first real-time end-to-end 40-Gb/s PAM-4 for next-generation access applications using 10-Gb/s transmitter," *J. Lightwave Technol.*, vol. 34, no. 7, pp. 1628–1635, 2016.

[10] J. Man, S. Fu, H. Zhang, J. Gao, L. Zeng, and X. Liu, "Downstream transmission of pre-distorted 25-Gb/s faster-than-Nyquist PON with 10G-class optics achieving over 31 dB link budget without optical amplification," in *Optical Fiber Communication Conf. and Exhibition (OFC)*, Anaheim, California, 2016.

[11] D. van Veen and V. Houtsma, "Symmetrical 25-Gb/s TDM-PON with 31.5-dB optical power budget using only off-the-shelf 10-Gb/s optical components," *J. Lightwave Technol.*, vol. 34, no. 7, pp. 1636–1642, 2016.

[12] M. Tao, L. Zhou, S. Yao, D. Zou, S. Li, H. Lin, and X. Liu, "28-Gb/s/λ TDM-PON with narrow filter compensation and enhanced FEC supporting 31.5 dB link loss budget after 20-km downstream transmission in the C-band," in *Optical Fiber Communication Conf. and Exhibition (OFC)*, Anaheim, California, 2016.

[13] V. Houtsma and D. van Veen, "A study of options for high-speed TDM-PON beyond 10G," *J. Lightwave Technol.*, vol. 35, no. 4, pp. 1059–1066, 2017.

[14] C. Sun, S. H. Bae, and H. Kim, "Transmission of 28-Gb/s duobinary and PAM-4 signals using DML for optical access network," *IEEE Photon. Technol. Lett.*, vol. 29, no. 1, pp. 130–133, 2017.

[15] D. van Veen and V. Houtsma, "Proposals for cost-effectively upgrading passive optical networks to a 25G line rate," *J. Lightwave Technol.*, vol. 35, no. 6, pp. 1180–1187, 2017.

[16] T. Minghui, L. Zhou, H. Zeng, S. Li, and X. Liu, "50-Gb/s/λ TDM-PON based on 10G DML and 10G APD supporting PR10 link loss budget after 20-km downstream transmission in the O-band," in *Optical Fiber Communication Conf. and Exhibition (OFC)*, Los Angeles, California, 2017.

[17] S. Yin, V. Houtsma, D. van Veen, and P. Vetter, "Optical amplified 40-Gbps symmetrical TDM-PON using 10-Gbps optics and DSP," *J. Lightwave Technol.*, vol. 35, no. 4, pp. 1067–1074, 2017.

[18] D. Liu and M. Tao, "50G single wavelength PON analysis and comparison," in *IEEE 802.3 NG-EPON Study Group Meeting*, Orlando, Florida, Nov. 2017 [Online]. Available: http://www.ieee802.org/3/ca/public/meeting_archive/2017/11/liu_3ca_2a_1117.pdf.

[19] A. Stark and T. Detwiler, "Equalization strategies for 25G PON," in *Optical Fiber Communication Conf. and Exhibition (OFC)*, Los Angeles, California, 2017.

[20] R. Bonk, W. Poehlmann, D. van Veen, J. Galaro, R. Farah, H. Schmuck, and T. Pfeiffer, "The underestimated challenges of burst-mode WDM transmission in TWDM-PON," *Opt. Fiber Technol.*, vol. 26, pp. 59–70, 2015.

[21] J. Rue, M. Itzler, N. Agrawal, S. Bay, and W. Sherry, "High performance 10 Gb/s PIN and APD optical receivers," in *Electronic Components and Technology Conf.*, San Diego, California, 1999, pp. 207–215.

[22] N. Duan, T.-Y. Liow, A. E.-J. Lim, L. Ding, and G. Q. Lo, "310 GHz gain-bandwidth product Ge/Si avalanche photodetector for 1550 nm light detection," *Opt. Express*, vol. 20, pp. 11031–11036, 2012.

[23] G. P. Agrawal, *Fiber-Optic Communication Systems*, 3rd ed. Wiley, 2002.

[24] J. G. Proakis, *Digital Communications*, 4th ed., McGraw-Hill, 2000.

[25] J. G. Proakis and D. G. Manolakis, *Digital Signal Processing. Principles, Algorithms, and Applications*, 4th ed. Prentice Hall, 1996.

[26] S. Bottacchi, *Theory and Design of Terabit Optical Fiber Transmission Systems.*, Cambridge University, 2014.

[27] G. L. Li, T. G. B. Mason, and P. K. L. Yu, "Analysis of segmented traveling-wave optical modulators," *J. Lightwave Technol.*, vol. 22, no. 7, pp. 1789–1796, 2004.

[28] Spectrolab, "043643: 10 Gb/s InGaAs/InAlAs avalanche photodetector (APD) die," 2017 [Online]: Available: http://www.spectrolab.com/sensors/pdfs/products/SR%20APD%2010G%20Die_RevA%20052512.pdf.

[29] Y. Kang, M. Zadka, S. Litski, G. Sarid, M. Morse, M. J. Paniccia, Y.-H. Kuo, J. Bowers, A. Beling, H.-D. Liu, D. C. McIntosh, J. Campbell, and A. Pauchard, "Epitaxially-grown Ge/Si avalanche photodiodes for 1.3 μm light detection," *Opt. Express*, vol. 16, pp. 9365–9371, 2008.

[30] F. Effenberger, "NRZ-NFC for 28G-PON," in *IEEE 802.3 NG-EPON Study Group Meeting*, Dallas, Texas, Nov. 2015 [Online]. Available: http://www.ieee802.org/3/NGEPONSG/public/2015_11/ngepon_1511_effenberger_3.pdf

[31] M. Chagnon, M. Osman, M. Poulin, C. Latrasse, J.-F. Gagné, Y. Painchaud, C. Paquet, S. Lessard, and D. Plant, "Experimental study of 112 Gb/s short reach transmission employing PAM formats and SiP intensity modulator at 1.3 μm," *Opt. Express*, vol. 22, pp. 21018–21036, 2014.

[32] A. Samani, M. Chagnon, D. Patel, V. Veerasubramanian, S. Ghosh, M. Osman, Q. Zhong, and D. V. Plant, "A low-voltage 35-GHz silicon photonic modulator-enabled 112-Gb/s transmission system," *IEEE Photon. J.*, vol. 7, no. 3, pp. 1–13, 2015.

[33] V. Houtsma, D. van Veen, A. Gnauck, and P. Iannone, "APD-based duobinary direct detection receivers for 40 Gbps TDM-PON," in *Optical Fiber Communications Conf. and Exhibition (OFC)*, Los Angeles, California, 2015.

[34] Z. Huang, C. Li, D. Liang, K. Yu, C. Santori, M. Fiorentino, W. Sorin, S. Palermo, and R. G. Beausoleil, "25 Gbps low-voltage waveguide Si-Ge avalanche photodiode," *Optica*, vol. 3, pp. 793–798, 2016.

[35] H. H. Lee, K.-H. Doo, S.-G. Mun, K. Kim, J. H. Lee, S.-K. Kang, H. Park, N. Park, H. Park, and H. S. Chung, "Real-time demonstration of QoS guaranteed 25-Gb/s PON prototype with Ethernet-PON MAC/PHY and cost-effective APD receivers for 100-Gb/s access networks," *Opt. Express*, vol. 24, pp. 13984–13991, 2016.

[36] M. Nada, M. Nakamura, and H. Matsuzaki, "25-Gbit/s burst-mode optical receiver using high-speed avalanche photodiode for 100-Gbit/s optical packet switching," *Opt. Express*, vol. 22, pp. 443–449, 2014.

Pablo Torres-Ferrera received B.E., M.E.E., and Ph.D. degrees (with honors) in Telecommunications in 2010, 2012, and 2017, respectively, from the National Autonomous University of Mexico (UNAM), Mexico City. He worked from 2012 to 2013 at Huawei Technologies Mexico in the implementation of OTN rings. As part of his Ph.D. investigation work, he carried out research internships at Athens Information Technology (AIT), Greece, in 2014 and at Politecnico di Torino, Italy, in 2016. He is currently a postdoctoral researcher at Politecnico di Torino, working in the field of high-speed optical access networks.

Valter Ferrero (M'97) received the Laurea degree (summa cum laude) in Electronics Engineering in 1994 from Politecnico di Torino, Italy. In 1994, he collaborated with Politecnico di Torino, working on coherent optical systems. From 1995 to 1996, he was with GEC Marconi, Genova, Italy. In 1997, he was in charge of the Optical Laboratory, Department of Electrical Engineering, Politecnico di Torino, and became Assistant Professor in 2001. He is currently with the Optical Communications Group, Politecnico di Torino. His current research interests include optical coherent communications, free-space optical communications, and next-generation passive optical networks.

Maurizio Valvo received a M.Sc. degree in Electronics Engineering cum laude at the University of Naples (Italy) in

1991. In the same year, he joined CSELT, the Telecommunications Research Centre and Laboratories, which is now TIM Lab–Turin and where he is currently active. He has focused since the beginning of his career on broadband access networks and, in particular, on PON systems, which he has also contributed to specify, develop, and test during the 1990s in the framework of several European-funded projects. He has led research projects with the objective to specify and test, both in the laboratory and in the field, innovative access network technologies based on PON, xDSL, HFC, Wimax, and free space optics. He currently leads the laboratory for fixed access network innovation and a research project for the innovation of the Telecom Italia optical access network. He holds four patents and is the co-author of three books and several papers.

Roberto Gaudino, Ph.D., is currently an associate professor at Politecnico di Torino, Italy. His main research interests are in long-haul DWDM systems, fiber nonlinearity, modeling of optical communication systems, and in the experimental implementation of optical networks, with a specific focus on access networks. In particular, in the last five years, he focused his activity on short-reach optical links using plastic optical fibers (POF) and on next-generation passive optical access networks (NG-PON2). Currently, he is working on ultra-high-capacity systems for medium-reach links. Previously, he worked extensively on fiber modeling, optical modulation formats, coherent optical detection, and on the experimental demonstration of packet-switched optical networks. He is the author or co-author of more than 200 papers in the field of optical communications. From 2009 to 2016, he was the coordinator of three projects in the area of optical access (EU FP6-IST STREP "POF-ALL" and "POF-PLUS" and EU FP7-ICT STREP project "FABULOUS"). He is now the coordinator of the PhotoNext center at POLITO.

Queries

1. AU: For Ref. [9], I have replaced the et al. with the names of the other authors based on this reference: https://www.osapublishing.org/jlt/abstract.cfm?uri=jlt-34-7-1628Please confirm that the change is correct.

2. AU: Please provide all the author names in place of “et al.” in ’Ref. [32]’ as per journal style requirement.

3. AU: For Ref. [32], I have added the author names, based on this reference:http://ieeexplore.ieee.org/document/7096918/authors?ctx=authorsPlease confirm that this change is correct.